Continuous Measurement of Atomic Force Microscope Tip Wear by Contact Resonance Force Microscopy

Jason P. Killgore, Roy H. Geiss, and Donna C. Hurley*

The atomic force microscope (AFM) continues to find increasing applications in nanoscale imaging,[1] metrology,[2] devices,[3] and manufacturing.[4] In these applications, tip size and shape critically affect the accuracy, resolution, and reliability of measurements and processes.[5] However, during tip–sample contact the tip can wear and break, undermining the utility of the instrument.[6] Thus, the development of wear-resistant probes, protocols for their testing and a fundamental understanding of their wear process is of vital importance. Although wear-resistant probes continue to advance,[7,8] tribological test methods and the collection of data for theoretical models still require measurements ex situ to the scanning process. Scanning electron microscopy (SEM)[8–12] and blind reconstruction while scanning on high-aspect-ratio reference samples[8,12,13] have both been used to correlate scanning history with tip geometry changes. Such ex-situ approaches are slow and can cause additional wear, fracture, and contamination. More recently, periodic force–displacement adhesion measurements have provided a less disruptive means of monitoring changes in contact area after scanning a finite distance.[8,11,12] Still, adhesion measurements require interruption of the scan, and quantitative determination of a contact radius can be strongly affected by geometry, contamination, and environmental conditions. Here, we demonstrate how contact resonance force microscopy (CR-FM) methods enable quantitative in-situ evaluation of tip wear by measurement of instantaneous changes in contact radius while scanning Si cantilevers on a Si substrate. It is found that CR-FM measurements do not adversely affect the wear process, and the results compare favorably with ex-situ techniques. Overall, CR-FM is shown to be an effective tool for detecting subnanometer changes in the contact radius while also revealing novel information about tip symmetry and wear rate.

Contact resonance force microscopy experiments and analysis are well described in the literature.[14] Briefly, an AFM tip is brought into contact with a sample, and the sample or cantilever is vibrated out of plane over a frequency range that excites a flexural resonance. Due to tip–sample interactions, the contact resonance of a given eigenmode will be shifted to higher frequencies compared to the free air resonance. We model the cantilever as a distributed-mass beam with cantilever spring constant k_L (see the Supporting Information (SI) for more details). One end is clamped at the cantilever holder, and a spring representing the tip–sample contact is located some finite distance from the beam's end. With this model, the contact stiffness k can then be determined from k_L and the free and contact resonance frequencies f_n^0 and f_n^c, respectively, of the nth eigenmode. Tip wear is measured by changes in the tip–sample contact radius a, which is related to k by[15]

$$k = 2a E^* \tag{1}$$

where E^* is the reduced elastic modulus of the tip–sample system. Assuming that the tip and sample mechanical properties do not change during measurement, E^* remains constant. Because f_n^0 is also constant, any changes in f_n^c during scanning on a homogeneous substrate can be unambiguously related to changes in a. If f_n^c is continuously monitored while scanning the cantilever and acquiring an AFM image, it is possible to measure changes in tip wear on a pixel-by-pixel basis with resolution in a limited only by the uncertainty with which f_n^c is measured.

Continuous monitoring of the contact resonance frequency f_n^c can be achieved through a number of recently developed CR-FM techniques.[16,17] Here we used dual AC resonance tracking (DART), because it allows for small drive amplitudes and provides high frequency resolution.[17] Force feedback in DART is identical to standard AFM contact mode, but DART also makes use of two low-amplitude sinusoidal excitations to track changes in f_n^c. During scanning, the total scan distance d is equal to two times the nominal scan length per line, times the number of scan lines, plus any overscan programmed into the raster pattern. Data are acquired as trace and retrace images, where each pixel represents a specific contact resonance frequency f_n^c and distance scanned d. The images are then unwrapped into a 1D array of measured f_n^c values, from which values of k and then a can be calculated.

An example of monitoring contact resonance frequency during scanning is shown in **Figure 1**. The frequency f_2^c of the second contact eigenmode increased from 963.3 ± 0.4 to 981.1 ± 0.4 kHz over a scanned distance d = 1.28 mm, corresponding to an increase in a as the tip wore. Because most wear studies are based on standard contact-mode scanning, we investigated whether frequency tracking interfered with the standard contact-mode wear mechanism and wear rate.

Dr. J. P. Killgore, Dr. R. H. Geiss, Dr. D. C. Hurley
Materials Reliability Division
National Institute of Standards and Technology
325 Broadway, Boulder, CO 80305, USA
E-mail: jason.killgore@nist.gov

DOI: 10.1002/smll.201002116

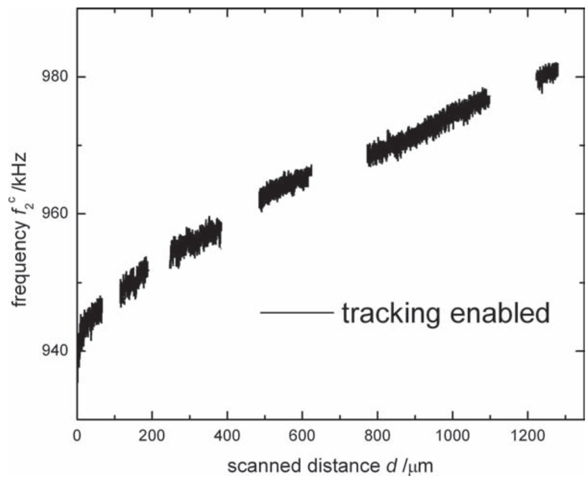

Figure 1. Second contact eigenmode f_2^c versus scanned distance d for a rectangular Si cantilever with $k_L = 2.38 \pm 0.05$ N m^{-1} scanned on a Si <100> substrate. DART frequency tracking and excitation were alternately enabled and disabled. Blank areas represent intervals when frequency tracking and cantilever excitation were disabled.

This was achieved by periodically enabling and disabling cantilever excitation and frequency tracking during scanning (i.e., the system alternates between DART and standard contact modes). For the regions in Figure 1 where tracking was enabled, f_2^c increased monotonically with d, corresponding to a progressive increase in contact radius. No tip wear information was recorded in the tracking-disabled regions, but interpolation between adjacent tracking-enabled regions indicates no significant change in the wear rate. This result contrasts with recent reports showing that fixed-frequency contact-resonance and near-contact-resonance excitation of AFM cantilevers can reduce or eliminate tip wear.[18] In our case, the minimal effect of tracking on tip wear is attributed to the small force modulation amplitudes used by DART. The contact stays within the linear elastic regime, because the force modulation represents only ≈1% of the applied static force. By comparison, the previously reported experiments showing reduced wear with near-resonance excitation intentionally drove the contact nonlinear. Thus, low-amplitude CR-FM appears to be a suitable tool for measuring in-situ tip wear in contact mode.

Figure 2 shows a comparison of in-situ CR-FM results with ex-situ measurements. Included are values of the contact radius determined by CR-FM and SEM (a_{CRFM} and a_{SEM}, respectively), values of the adhesion force F_{adh} determined by force-displacement methods,[19] and SEM images of the tip with radius of curvature R indicated. All measurements were made with a stiff cantilever with spring constant $k_L = 48 \pm 5$ N m^{-1}. CR-FM measurements were made by tracking the first contact eigenmode frequency f_1^c while scanning at a speed of 1.25 μm s^{-1}. The results were obtained before, during or after the following measurement steps: i) SEM characterization of the as-manufactured AFM tip; ii) the tip was brought into contact and subjected to an applied force F_{app} = 2 μN; iii) the tip was scanned for a distance d = 0.59 mm with F_{app} = 610 nN; and iv) the tip was scanned an additional d = 3.56 mm with F_{app} = 469 nN. Frequency tracking was enabled throughout steps (iii) and (iv). After steps (ii), (iii), and (iv), the tip was removed from the AFM and imaged by SEM. In addition, the adhesion force F_{adh} was measured after step (ii), at the start and finish of step (iii) and after step (iv).

From the SEM image in Figure 2b, it can be seen that the new tip forms an extremely sharp apex (typical radius of curvature R < 7 nm according to manufacturer). Consistent with earlier reports, Figures 2b,c reveal that initial contact at relatively high forces leads to significant material loss and

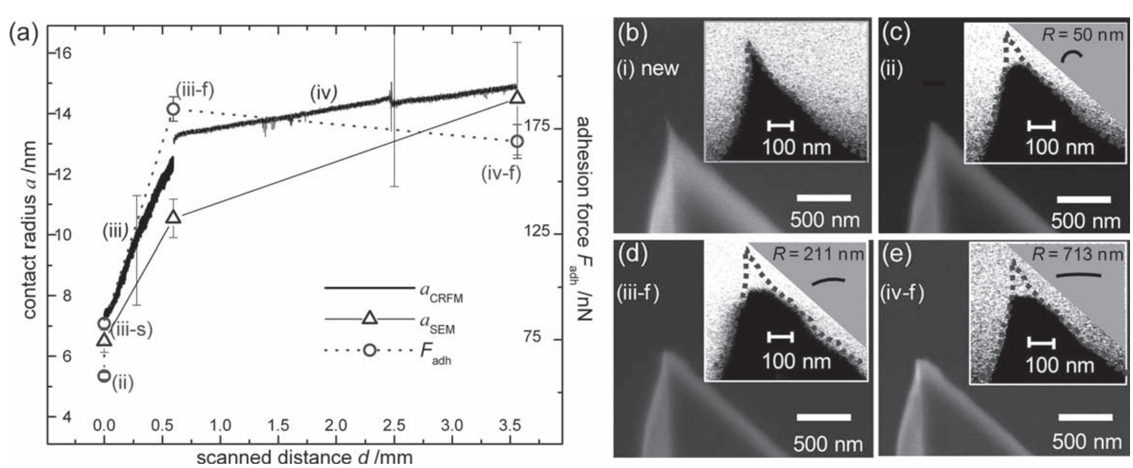

Figure 2. Combined in-situ and ex-situ tip wear data acquired with a rectangular Si cantilever with $k_L = 48 \pm 5$ N m^{-1} scanned on a Si <100> substrate. Data were acquired i) when the tip was new, ii) after initial F_{app} = 2 μN contact with substrate, iii) while scanning 0.59 mm at F_{app} = 610 nN, and iv) while scanning an additional 3.56 mm at F_{app} = 469 nN. Suffixes "s" and "f" denote the start and finish of the scanning steps. AFM data in (a) includes the in-situ contact radius a_{CRFM} determined by tracking the first contact eigenmode f_1^c and the adhesion force F_{adh} determined from force–displacement measurements. Uncertainty in a_{CRFM} is shown for two representative points. Panels (b–e) are SEM images of the AFM tip b) when new, c) after step (ii), d) after step (iii), and e) after step (iv). Inset images have been color-inverted and thresholded for clarity. An overlay of the original tip shape is added to provide guidance for assessing the extent of tip wear. The arcs in (c–e) represent a best fit of a semicircle of radius R to the tip apex. The values of contact radius a_{SEM} determined from these values of R are included in (a).

blunting of the tip.[20] This change was attributed to yielding and failure from the high stresses introduced by high-force contact with the rigid Si substrate. Figures 2c–e show that scanning continued to progressively blunt the tip. By fitting the tip apex in the SEM micrograph to a semicircular arc of radius R and applying a hemispherical Hertzian contact model, the contact radius a_{SEM} was estimated for a given applied load. The fitted radii of curvature are also shown in Figures 2c–e. The calculated contact radii are summarized in Figure 2a. The a_{SEM} was calculated to increase from 6.5 ± 0.4 nm after step (ii) to 14.5 ± 1.9 nm after step (iv).

In Figure 2a, it can be seen that the CR-FM measurements allowed continuous quantification of the changes in a throughout the scan. Scanning in step (iii) resulted in a 70% increase in a_{CRFM} from 7.3 ± 1.3 to 12.4 ± 2.3 nm. Scanning in step (iv) resulted in an additional 14% increase in a_{CRFM} from 13.1 ± 2.4 to 14.9 ± 2.9 nm. At the start of (iii) and the end of (iv), a_{CRFM} shows good agreement with a_{SEM}. At the end of (iii), a_{CRFM} was higher than a_{SEM} but still within the CR-FM uncertainty. The discrepancy likely originated from the difficulty in ascribing an accurate radius of curvature to the irregular blunted tip. The observed 15-25% uncertainties in the CR-FM-measured contact radii are absolute and were determined by propagating the uncertainties in frequency, spring constant, tip position, and material properties. In addition, the precision or resolution of the technique, which refers to the ability to detect small relative changes in a, was determined from the frequency scatter in a single scan line. Here, typical values were less than 0.05 nm (less than 1%), and are indicative of the high resolution in a provided by CR-FM.

Also shown in Figure 2a are measurements of adhesion force F_{adh}, which are expected to correlate with the changes in a measured by CR-FM. An accurate determination of contact radius from F_{adh} depends on knowledge of the tip-sample work of adhesion, the tip geometry, and whether the system is better described by a Derjaguin–Mueller–Toporov (DMT) or a Johnson–Kendall–Roberts (JKR) contact mechanics model.[21] Such analysis was outside the scope of this communication. Still, with constant material properties and environmental conditions the work of adhesion should remain constant, and changes in F_{adh} should scale monotonically with changes in a.[8,11,12] From Figure 2a, F_{adh} increased 123% from 83 ± 2 to 184 ± 6 nN during step (iii). From the end of step (iii) to the end of step (iv), F_{adh} showed a slight decrease from 184 ± 6 to 169 ± 8 nN. Overall, from the start of step (iii) to the end of step (iv), both a_{CRFM} and F_{adh} increased 104%, showing excellent quantitative agreement. The discrepancy between a_{CRFM} and F_{adh} for the intermediate steps may have resulted from changing environmental conditions or SEM induced tip contamination. Indeed, repeating the same experiments without ex-situ SEM showed consistently good agreement between relative changes in a and relative changes in F_{adh} (SI, Figure S3). Finally, the CR-FM data in Figure 2a also show an inconsistency with the expected behavior. Between steps (iii) and (iv), repositioning of the cantilever in the holder resulted in an unintentional decrease in F_{app} from 610 to 469 nN. A decrease in F_{app} should have resulted in a decreased a, but instead a sharp increase in a was observed at the beginning of step (iv). This jump indicates a potential drawback of ex-situ measurements, namely that one or more of the external measurements affected the tip geometry.

Many contact-mode AFM experiments, particularly those studying tribology, seek to minimize applied forces by using more compliant cantilevers than discussed above. A benefit to using CR-FM to detect in-situ changes in contact radius is that the stiffness sensitivity, and hence sensitivity to changes in a, can be tailored by the choice of eigenmode used for monitoring.[22] With force–distance and subresonance modulation techniques, stiffness sensitivity is typically greatest when the contact stiffness k is less than, or comparable to, the cantilever spring constant k_{L}.[19] In CR-FM, the use of higher-order resonance modes enables sensitive measurement of k even when it is many orders of magnitude larger than k_{L}, allowing the study of tip wear with compliant cantilevers on a rigid substrate. This was demonstrated by scanning a compliant Si cantilever with $k_L = 0.11 \pm 0.005$ N m^{-1} for $d = 590$ μm on a Si substrate with $F_{\mathrm{app}} = 1.2$ nN. Point contact resonance spectra acquired before and after scanning showed an increase in the first contact eigenmode f_1^c of only 0.5 ± 0.1 kHz, from 47.6 to 48.1 kHz. In contrast, the enhanced sensitivity of the fourth contact eigenmode f_4^c showed an increase of 54.6 ± 0.1 kHz, from 416.1 to 470.7 kHz. This enhanced sensitivity revealed a considerable richness of wear information when f_4^c was tracked in situ, as shown in **Figure 3**.

Compared to the data in Figure 2, the low forces used to obtain Figure 3 resulted in much smaller initial values of the contact radius (<1 nm, compared to >7 nm in Figure 2). The low-force wear behavior of such a sharp probe showed greater complexity compared to the dulled probe in Figure 2. From the plot, five distinct wear regions were identified for this particular cantilever. Upon initial scanning,

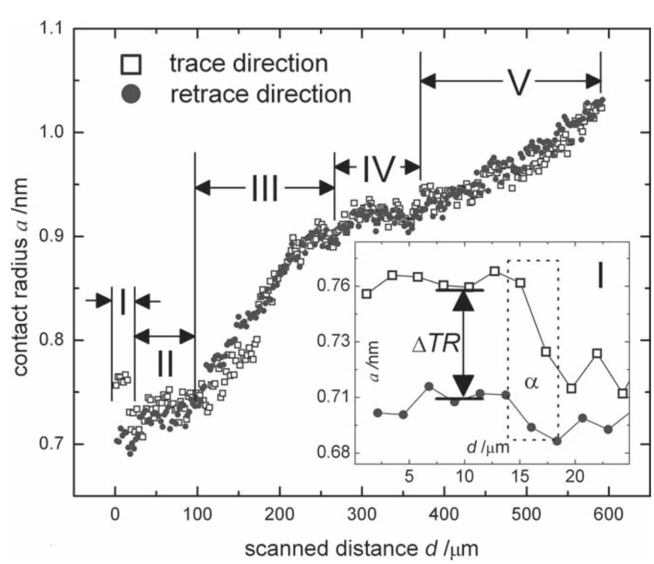

Figure 3. Contact radius ***a*** versus scanned distance ***d*** for a rectangular Si cantilever with $k_{\mathrm{L}} = 0.11 \pm 0.005$ N m^{-1} scanned on a Si <100> substrate with $F_{\mathrm{app}} = 1.2$ nN. Data were acquired by tracking the fourth contact eigenmode frequency f_4^c. Regions I through V designate specific tip-shape and tip-wear behaviors described in the text. The inset shows a magnified view of region I. ΔTR is the calculated difference in contact radius between the trace and retrace scan directions. α indicates a rapid change in a, attributed to tip breakage.

Table 1. Measured and calculated properties of cantilevers used in this study.

Related figure	Cantilever spring constant k_L [N m^{-1}]	Eigenmode tracked n	nth free resonance f_n^0 [kHz]	Calculated tip position γ
1	2.38 ± 0.05	2	454.7	N/A
2	48 ± 5	1	172.5	1.00
3	0.11 ± 0.005	4	363.2	0.90

region I contained distinctly different average values of a for the forward-trace and backward-retrace scan directions. This trace–retrace difference ΔTR was attributed to asymmetry of the tip. The asymmetry was observed because friction forces induce torsional bending of the cantilever and expose the contact to slightly different aspects of the tip. This region of pronounced asymmetry remained consistent for ≈15 µm of scanning. Towards the end of region I, a rapid change in a denoted by α was observed. α was attributed to tip breakage and resulted in a reduced ΔTR value and hence increased tip symmetry. In region II, a remained metastable up to $d \approx 90$ µm. In region III, a increased progressively, while ΔTR was continually reduced. The wear rate gradually slowed around $d \approx 250$ µm, leading to a second metastable plateau (region IV). Finally, the wear process was reinitiated in region V. The existence of metastable plateaus in regions II and IV suggests the occurrence of complex tribochemical processes, although their precise mechanisms are outside the scope of this letter. More importantly, the results highlight the ability of CR-FM to resolve small changes in contact radius, even for very sharp probes and low applied forces.

At present, one limitation of CR-FM is that it cannot evaluate wear-induced volume changes in the tip, as has been done with SEM and TEM imaging.[8,9,12] However, volume information might be gained by periodically measuring the force dependence of the contact radius in order to reconstruct the tip's axisymmetric geometry.[23] Changes in tip volume could then be inferred by comparing the reconstructed geometry to a single SEM or TEM image acquired at the start of the experiment.

In summary, we have demonstrated that contact resonance force microscopy provides a new platform to study tip wear for a broad range of cantilever stiffnesses and applied loads, without the need to perform disruptive ex-situ experiments. By measuring changes in contact resonance frequency and relating them to changes in contact radius, tip changes are observed in real time during scanning. Our approach to measuring tip wear in situ should lend valuable insight to the study of nanoscale and single-asperity-contact wear mechanisms. For example, our approach provides unique access to tip wear information at very short scan distances, allowing investigation of the onset of wear. Further, in-situ CR-FM measurement of tip wear has important industrial applications. CR-FM could be used as a means to continuously monitor tip wear in tip-based manufacturing processes. Also, periodic acquisitions of point contact resonance spectra could be implemented to monitor tip sharpness in AFM-based dimensional metrology without significant modifications of the instrumentation. Finally, the ability to measure contact radius during scanning has implications for more general fundamental studies on friction and contact mechanics.

Experimental Section

Sample Preparation: All measurements were performed on a silicon <100> substrate. Prior to CR-FM experiments, the Si wafer was rinsed with acetone, methanol, and isopropanol, then sonicated in a 1:1 ethanol:water mixture. Following sonication, the wafer was rinsed with ethanol, then placed in a ultraviolet ozone cleaner for 15 min.

Cantilever Selection and Properties: The properties of the three AFM cantilevers used in these experiments are summarized in **Table 1**. The cantilever spring constant k_L was determined with the AFM's built-in thermal calibration. The free resonance frequencies f_n^0 were measured from resonance spectra obtained with the instrument's built-in lock-in amplifier. The relative position γ of the tip along the cantilever was determined from point contact resonance spectra acquired after the wear tests. Spectra were acquired for the nth eigenmode, which was tracked during wear testing, and the n+1th (in Figure 2) or n-1th (in Figure 3) eigenmodes. The value of γ was determined by calculating contact stiffness as a function of γ for the two adjacent eigenmodes, then choosing the value of γ where the two modes gave identical results.[14]

AFM Measurements: All AFM measurements were made in ambient environmental conditions (temperature = 18 °C, relative humidity = 40%). CR-FM measurements were performed with the internal DART functionality of the MFP-3D AFM (Asylum Research, Santa Barbara, CA).[24] The Si sample was glued to a commercial ultrasonic transducer with a broadband resonance at ≈1 MHz (Parametrics V103, Olympus, Waltham, MA). The transducer drive amplitudes ranged from 10 to 50 mV, yielding a contact resonance amplitude of ≈1 mV as determined by the lock-in amplifier. The data for Figure 1 were acquired by continuously scanning a 1 µm × 0.5 µm region with 128 lines of resolution. The data for Figure 2 were acquired by first scanning a 1 µm × 1 µm region with 256 lines of resolution, followed by a new 5 µm × 5 µm region with 256 lines of resolution. The data for Figure 3 were acquired by scanning a 1 µm × 1 µm region with 256 lines of resolution. For all measurements, fast-scanning was performed perpendicular to the long axis of the cantilever at a scan velocity of 1.25 µm s^{-1}. Adhesion force F_{adh} measurements in Figure 2 were performed with the AFM's force–distance panel, with three F_{adh} measurements taken at each measurement step.

SEM Characterization: Prior to each SEM imaging step, the cantilever was transferred from the MFP-3D cantilever holder to a custom SEM cantilever holder. SEM images were obtained at magnifications from 100 000× to 200 000× with beam voltages from 3 to 10 kV. a_{SEM} was determined by tracing the tip apex and fitting the trace to semicircle of radius R (SI, Figure S2). R was then used in a Hertzian contact model to determine a_{SEM}.

Supporting Information

Supporting Information is available from the Wiley Online Library or from the author.

Acknowledgements

The authors thank Dr. Bernd Gotsmann (IBM Zürich) for informative discussions. This research was performed while JPK held a National Research Council Research Associateship Award at the National Institute of Standards and Technology. This official contribution of the National Institute of Standards and Technology is not subject to copyright in the United States.

[1] F. J. Giessibl, *Rev. Mod. Phys.* **2003**, *75*, 949.
[2] D. J. Whitehouse, *Contemp. Phys.* **2008**, *49*, 351.
[3] P. Vettiger, M. Despont, U. Drechsler, U. Duerig, W. Haberle, M. I. Lutwyche, H. E. Rothuizen, R. Stutz, R. Widmer, G. K. Binnig, *IBM J. Res. Dev.* **2000**, *44*, 323.
[4] a) K. Salaita, Y. H. Wang, C. A. Mirkin, *Nat. Nanotechnol.* **2007**, *2*, 145; b) M. Hirtz, M. K. Brinks, S. Miele, A. Studer, H. Fuchs, L. Chi, *Small* **2009**, *5*, 919; c) Y. Wang, X. Hong, J. Zeng, B. Liu, B. Guo, H. Yan, *Small* **2009**, *5*, 477.
[5] A. Yacoot, L. Koenders, *J. Phys. D—Appl. Phys.* **2008**, *41*, 46.
[6] R. W. Carpick, M. Salmeron, *Chem. Rev.* **1997**, *97*, 1163.
[7] H. Bhaskaran, B. Gotsmann, A. Sebastian, U. Drechsler, M. A. Lantz, M. Despont, P. Jaroenapibal, R. W. Carpick, Y. Chen, K. Sridharan, *Nat. Nanotechnol.* **2010**, *5*, 181.
[8] J. Liu, D. S. Grierson, N. Moldovan, J. Notbohm, S. Li, P. Jaroenapibal, S. D. O'Connor, A. V. Sumant, N. Neelakantan, J. A. Carlisle, K. T. Turner, R. W. Carpick, *Small* **2010**, *6*, 1140.
[9] R. Agrawal, N. Moldovan, H. D. Espinosa, *J. Appl. Phys.* **2009**, *106*, 6.
[10] K. H. Chung, D. E. Kim, *Tribol. Lett.* **2003**, *15*, 135.
[11] B. Gotsmann, M. A. Lantz, *Phys. Rev. Lett.* **2008**, *101*, 4.
[12] J. J. Liu, J. K. Notbohm, R. W. Carpick, K. T. Turner, *ACS Nano* **2010**, *4*, 3763.
[13] W. Maw, F. Stevens, S. C. Langford, J. T. Dickinson, *J. Appl. Phys.* **2002**, *92*, 5103.
[14] a) U. Rabe, S. Amelio, E. Kester, V. Scherer, S. Hirsekorn, W. Arnold, *Ultrasonics* **2000**, *38*, 430; b) U. Rabe, in *Applied Scanning Probe Methods Vol. II*, (Eds: B. Bushan, H. Fuchs), Springer-Verlag, Berlin **2006**, *37*; D. C. Hurley, in *Applied Scanning Probe Methods Vol. XI*, (Eds: B. Bushan, H. Fuchs), Springer-Verlag, Berlin **2009**, 97.
[15] G. M. Pharr, W. C. Oliver, F. R. Brotzen, *J. Mater. Res.* **1992**, *7*, 613.
[16] a) K. Kobayashi, H. Yamada, K. Matsushige, *Surf. Interface Anal.* **2002**, *33*, 89; b) S. Jesse, S. V. Kalinin, R. Proksch, A. P. Baddorf, B. J. Rodriguez, *Nanotechnology* **2007**, *18*, 8; c) A. B. Kos, D. C. Hurley, *Meas. Sci. Technol.* **2008**, *19*, 015504; d) P. Steiner, R. Roth, E. Gnecco, T. Glatzel, A. Baratoff, E. Meyer, *Nanotechnology* **2009**, *20*, 6.
[17] B. J. Rodriguez, C. Callahan, S. V. Kalinin, R. Proksch, *Nanotechnology* **2007**, *18*, 6.
[18] a) M. A. Lantz, D. Wiesmann, B. Gotsmann, *Nat. Nanotechnol.* **2009**, *4*, 586; b) A. Knoll, H. Rothuizen, B. Gotsmann, U. Duerig, *Nanotechnology* **2010**, *21*, 8.
[19] H. J. Butt, B. Cappella, M. Kappl, *Surf. Sci. Rep.* **2005**, *59*, 1.
[20] M. Kopycinska-Müller, R. H. Geiss, D. C. Hurley, *Ultramicroscopy* **2006**, *106*, 466.
[21] K. L. Johnson, *Contact Mechanics*, Cambridge University Press, Cambridge**1985**.
[22] J. A. Turner, J. S. Wiehn, *Nanotechnology* **2001**, *12*, 322.
[23] K. Yamanaka, A. Noguchi, T. Tsuji, T. Koike, T. Goto, *Surf. Interface Anal.* **1999**, *27*, 600.
[24] Commercial equipment, instruments, or materials are identified only in order to adequately specify certain procedures. In no case does such identification imply recommendation or endorsement by the National Institute of Standards and Technology, nor does it imply that the products identified are necessarily the best available for the purpose.

Received: November 24, 2010
Revised: January 7, 2011
Published online: March 15, 2011